Narrow-Band Terahertz Waveform Generation in Periodically-Poled Lithium Niobate

T. Meade, Y.-S. Lee, V. Perlin, H. Winful, T.B. Norris
Center for Ultrafast Optical Science, University of Michigan, Ann Arbor, MI 48109-2099

A. Galvanauskas
IMRA America, 1044 Woodridge Ave., Ann Arbor, MI 48105

Abstract: We demonstrate a method for generation of narrow bandwidth THz fields by optical rectification, a nonlinear interaction between a 150-femtosecond optical pulse and a periodically-poled lithium niobate crystal. We present time-domain measurements of both amplitude and phase of the THz electric field, along with power spectra. At low temperature (13 K), the signal from a 1.2 mm long crystal is peaked at 1.80 THz with a bandwidth (FWHM) of 0.07 THz; the THz power is approximately 1.5 μW. Optical rectification in PPLN could provide a useful source field for characterization of THz sensors.

1. Nonlinear optics

The field of nonlinear optics is considered to have begun with the experiment by Franken *et al*. in 1961, in which the optical harmonic (second harmonic generation — SHG) of a ruby laser was produced by nonlinear interaction with a quartz crystal [1]. By nonlinear optics we mean that the interaction between the optical field and the medium, typically a crystal, depends on the field strength in a nonlinear manner. One generally creates nonlinear fields by inducing a nonlinear polarization in the crystal with a strong optical field and measuring the radiation emitted by the decay of the polarization.

In traditional, linear optics, the polarization induced in a medium is proportional to the electric field incident on the medium. This is expressed in the equation P = _ E. However, with the advent of lasers, and in particular, short-pulsed lasers, electric fields sufficiently large so that linear polarization approximation fails are easily attained. In general, therefore, one must expand the polarization as a power series in the applied field:

$$P = \chi^{(1)}E + \chi^{(2)}E^2 + \chi^{(3)}E^3 + \mathrm{L} \;= P^{(1)} + P^{(2)} + P^{(3)} + \mathrm{L} \qquad (1)$$

The term proportional to E gives the familiar linear polarization. In this paper, we are primarily interested in the second-order term, $P^{(2)}$. This term is responsible for such effects as second-harmonic generation, sum- and difference-frequency generation, parametric amplification and oscillation, and optical rectification.

As a concrete example of a second-order nonlinear effect, we will briefly examine difference frequency generation. We represent two fields as $E_1 = A_1 \exp[i\_1 t]$ and $E_2 = A_2 \exp[i\_2 t]$. Consider the polarization arising from the mixing of E_1 with E_2*:

$$P^{(2)} = \chi^{(2)} A_1 \exp[+i\omega_1 t] A_2^* \exp[-i\omega_2 t] = \chi^{(2)} (A_1 A_2^*) \exp[i(\omega_1 - \omega_2)t] \qquad (2)$$

It is immediately evident that the polarization oscillates with the difference frequency _ = _1 - _2. This polarization acts as a source term in the wave equation:

$$\left(\nabla^2 - \frac{1}{c^2}\frac{\partial^2}{\partial t^2}\right)E(z,t) = -\mu_0 \frac{\partial^2 P(z,t)}{\partial t^2}, \tag{3}$$

and we see that, because of the induced nonlinear polarization, there exists a radiated field at the difference frequency between the two applied fields [2,3]. Other second-order nonlinear interactions are, of course, possible. In the laboratory, a specific orientation of a nonlinear crystal will usually favor only one type of interaction.

The nonlinearity of specific interest to us is optical rectification, which one may think of simply as the degenerate case of difference frequency generation [4]. In optical rectification, the two fields come from the same laser. For a continuous-wave laser, the effect of the polarization is to induce a static DC voltage inside the crystal. Since the second derivative of such a polarization is zero, this term gives no radiation in the far-field. The case is very different for short-pulsed lasers. If the two fields in equation (2) come from the same pulse, then our expression for the polarization simplifies to:

$$P^{(2)}(t) = \chi^{(2)}[A(t)A^*(t)] = \chi^{(2)} I(t), \tag{4}$$

where $I(t)$ is the optical pulse s intensity profile. The net effect is to strip away the rapidly varying (~ 10^{15} Hz) optical carrier frequency, and leave only the relatively slowly varying (~ 10^{12} Hz) pulse envelope.

For pulses on the order of 100 femtoseconds, this corresponds to a polarization changing on sub-picosecond time-scales. If we prefer to visualize this process in the frequency domain, we may consider that a 100-femtosecond optical pulse has a spectrum on the order of a few terahertz (THz), and therefore terahertz frequencies may be generated if the optical pulse spectrum is sufficiently broad to support difference frequency generation between different spectral components of the same pulse.

For generating short bursts of coherent THz frequency light, a widely applied method is optical rectification in a velocity-matched medium. To maximize conversion efficiency, the optical pulse should travel with the same speed through the crystal as the THz wave, i.e. the group velocity of the optical pulse should be equal to the phase velocity of the THz wave. Under this condition, the forward-propagating THz wavefronts from different parts of the crystal interfere constructively, and at the output of the crystal, a substantial THz field is emitted. The radiated THz field has a peak frequency on the order of 1 THz, is extremely broad-band (_f ~ 1-2 THz), and consists of a single- or few-cycle pulse. The most common means of achieving this are with a pulsed laser operating around 800 nm and a <110> ZnTe crystal [5].

In lithium niobate, the optical group velocity is larger than the THz phase velocity, and so the two beams walk-off each other as they propagate through the crystal. The optical beam leads the THz beam by one optical pulse-length after a walk-off length

$$l_w = \frac{c\tau_p}{n_{THz} - n_{opt}} \tag{5}$$

In equation (5), τ_p is the optical pulse duration, n_{THz} and n_{opt} are the phase and group indices of the THz and optical fields, respectively, and c is the vacuum speed of light. For crystals significantly longer than l_w, only the front and back surfaces produce polarizations which contribute to the far-field THz field; everywhere else in the crystal, the polarization is constant and therefore nonradiative [6].

In a velocity-matched medium, it is clear that a long crystal corresponds to a large interaction length, which enables the generation of strong THz fields. In a medium with a velocity mismatch, the effective interaction length is the walk-off length. A crystal longer than the walk-off length is inefficient, since most of the polarization induced will be nonradiative. To generate a strong THz field, we use quasi-phase matching in a velocity-mismatched medium to circumvent this defect. We discuss these ideas in the following section.

2. Periodically-poled lithium niobate

Ferroelectric molecules such as lithium niobate (LN) possess a non-zero electric dipole moment even in the absence of an applied field. An edge perpendicular to the domain of a unipolar LN crystal is patterned with a photoresist grating of the desired domain structure. This edge is then covered with a thin metal film. A large (~ 20 kV/mm) field is applied, which is sufficient to reverse the polarity of the domains where the metal makes contact with the LN crystal, but is not strong enough to affect the domains below the photoresist layer [7].

Because the direction of a domain is a manifestation of the orientation of the molecules within a domain, for optical purposes, it is convenient to think of poling as directing the orientation of the crystal s optic axis. Domains that are anti-parallel have opposite sign nonlinear susceptibilities, $\chi^{(2)}$. In bulk PPLN, one domain in the crystal generates a THz pulse with the opposite polarity as the previous domain. This is shown schematically in figure 1. If the domain lengths are approximately equal to the walk-off length, the radiated THz fields from neighboring domains will connect smoothly and have a narrow spectrum centered about

$$f_f = \frac{c}{2l_d(n_{THz} - n_{opt})}. \tag{6}$$

Our effective interaction length therefore increases from the walk-off length to the entire length of the crystal. In our experiments, this increase is approximately a factor of 40 (see section 3). By generating a polarization through many domains of the crystal, we are able to generate a multi-cycle THz waveform, whose structure is determined mainly by the domain structure of the crystal. If the domains of a periodically-poled crystal reverse polarity on a scale $\Lambda_d \cong \Lambda_w$, then radiated field due to optical rectification is essentially a convolution of the crystal s domain structure with the pulse intensity envelope [8].

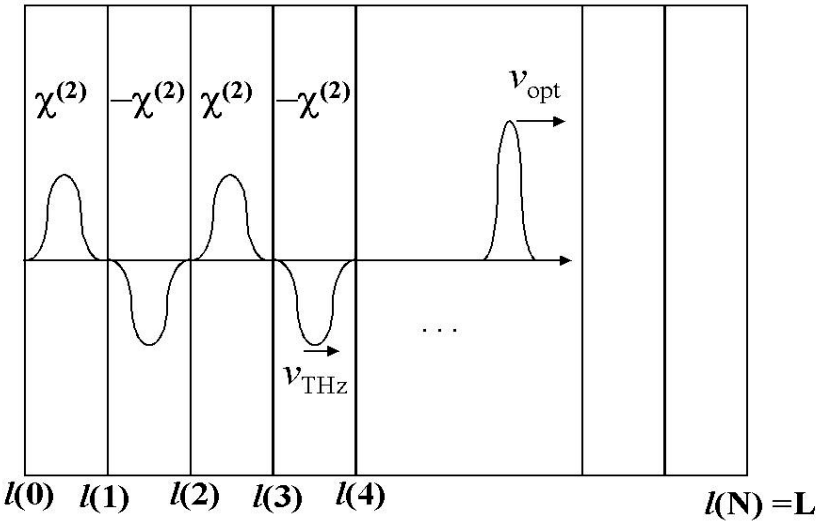

Fig. 1: Schematic diagram of the nonlinear polarization induced in the PPLN crystal.

3. Experimental procedure and results

A schematic of our experiment is shown in figure 2. In the figure, THz beams are shown as dotted lines, and optical beams are solid lines. The laser source for the experiments is a Ti:Sapphire regenerative amplifier, which produces 150-fs pulses at 800 nm with a repetition rate of 250 kHz [9]. The index of refraction over a broad range of THz frequencies has been measured to be approximately 5.2 [10]; we measured the optical group index to be 2.3 at room temperature. Using these values and our laser pulse duration in equation (5), we calculated a walk-off distance of approximately 24 microns in the crystal. We therefore chose a z-cut PPLN crystal, 1.2 mm long with a domain length of 30 microns for this work. The pulse energy incident on the sample is 400 nJ, focused to a spot size of roughly 100 microns. This signal beam was modulated at 50 kHz for lock-in amplifier detection. An off-axis parabolic mirror collimated the THz radiation from the PPLN. We measured the THz signal by electro-optic sampling. An optical probe pulse with a known polarizaton state co-propagated with the THz pulse. A second off-axis parabolic mirror focused both the probe and THz pulses onto a 1-mm thick, <110> ZnTe sensor crystal.

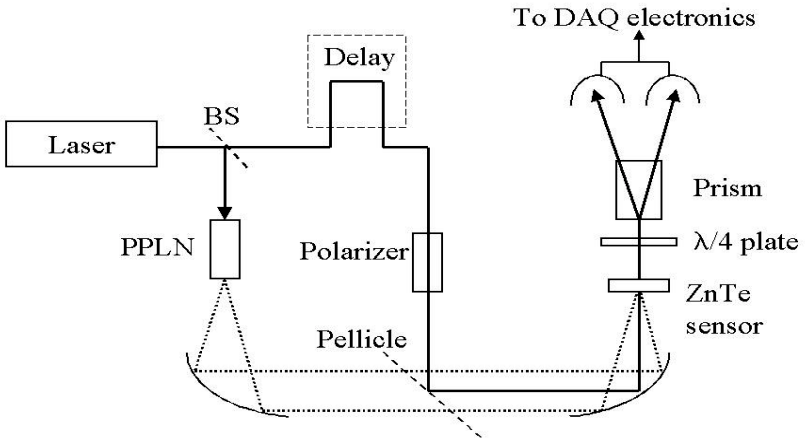

Fig. 2: Experimental set-up.

Free-space electro-optic sampling (FS-EOS) is an extension of conventional electro-optic sampling techniques used for characterizing local electric fields [11-13]. This method provides a means to measure the amplitude and phase of the THz field over a broad detection bandwidth. The main idea of FS-EOS is that the THz field modulates the optical properties of a crystal, and that modulation is probed with an optical beam. The THz electric field induces a birefringence in the sensor crystal, which in turn causes a phase retardation in the optical pulse. The phase retardation is proportional to the THz field strength, and gives a change in the polarization state of the optical beam. We measured the THz field strength by measuring the amount of polarization rotation in the optical probe beam with a pair of balanced photodiodes. Because of the excellent velocity matching between the THz and optical pulses in ZnTe, we can achieve ~ 200 femtosecond resolution of the THz pulse [14].

In figure 3(a), we show the THz waveform at room temperature, and in figure 3(b), its power spectrum. The main features of the signal are oscillations under an exponentially decaying envelope. At room temperature, we measure a peak frequency of 1.67 THz, with a bandwidth (FWHM) of 0.13 THz. Because the THz wave propagates through the crystal more slowly than the optical beam, smaller time delays correspond to signal emitted from near the back surface of the crystal, while larger time delays correspond to the part of the signal from closer to the front surface of the crystal. The emitted field from the back end of the crystal is significantly larger than that from the front end. We see that our main limitation at room temperature is absorption of the THz wave as it propagates through the PPLN crystal. The absorption loss due to phonons is expected to reduce at lower temperatures [15].

To reduce the absorption loss, we performed the same experiment with the PPLN crystal at 13 K. As shown in our time trace of the waveform, figure 3(c), absorption essentially vanishes at low temperatures. Figure 3(d) is the power spectrum at low temperatures, from which we measure a peak frequency of 1.80 THz and a bandwidth of 0.07 THz. We can attribute the discrepancy between the peak frequencies at low and room temperatures to several factors. At low temperatures, the crystal shrinks and so our domain lengths shorten, which increases our peak frequency. Also, the real parts of the indices of refraction may have some temperature dependence.

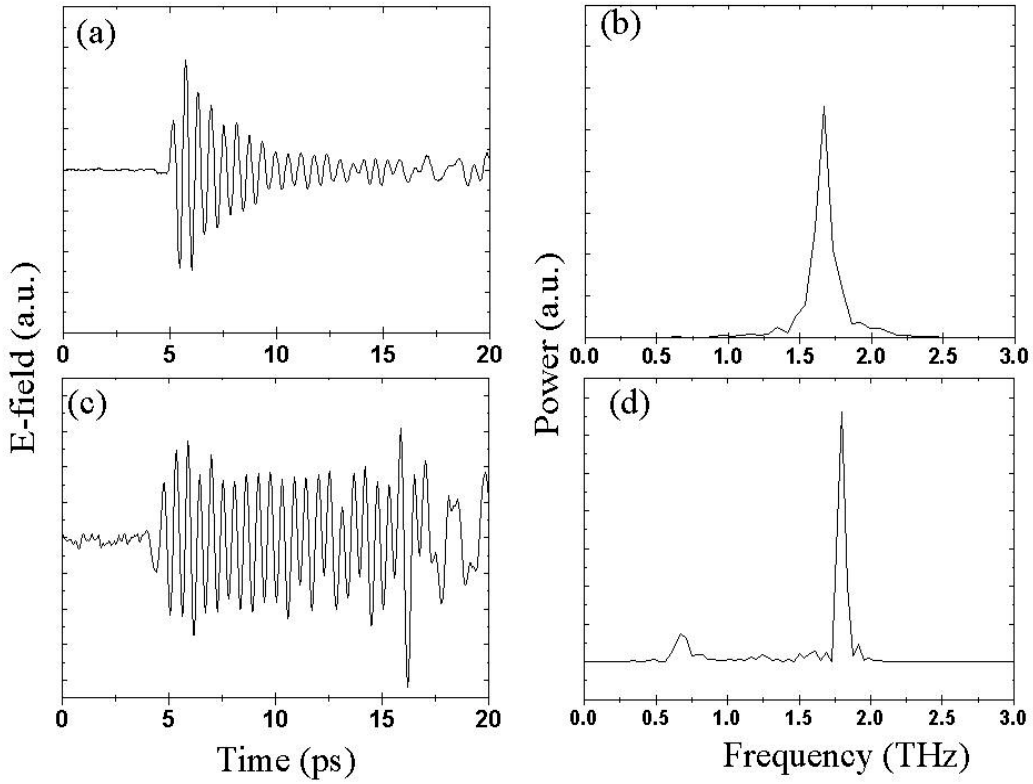

Figure 3: Time traces and power spectra of the THz field at room temperatures (a, b), and 13 K, (c, d).

To generate even narrower bandwidth fields, we tested a 7.2 mm PPLN crystal, with 30 micron domain lengths. At 18 K, this crystal generated 1.81 THz radiation with a bandwidth of 18 GHz (data not shown).

It is interesting to examine one of our room temperature scans over a large time window, as in figure 4(a). What we find is that the oscillations do not finish in a simple manner. After the exponential envelope has decayed, a beat pattern arises. This is a result of a counter-propagating THz polarization in the crystal. When the optical beam reflects off the back surface of the crystal, it induces a polarization which propagates in the opposite direction as the optical beam. This signal has a peak frequency of

$$f_b = \frac{c}{2l_d(n_{THz} + n_{opt})} \tag{7}$$

and lags the co-propagating signal in time. To see this effect more clearly, we can produce a time-frequency spectrogram of figure 4(b). Figure 4(b) is a wavelet decomposition of our signal with a Morlet basis [16,17]. At early times, we see the co-propagating signal, followed by both the counter-propagating signal, and a reflection of the co-propagating signal. The low frequency wave is peaked at 0.67 THz, with a bandwidth of 0.03 THz. Detailed measurements of this low-frequency wave await further study.

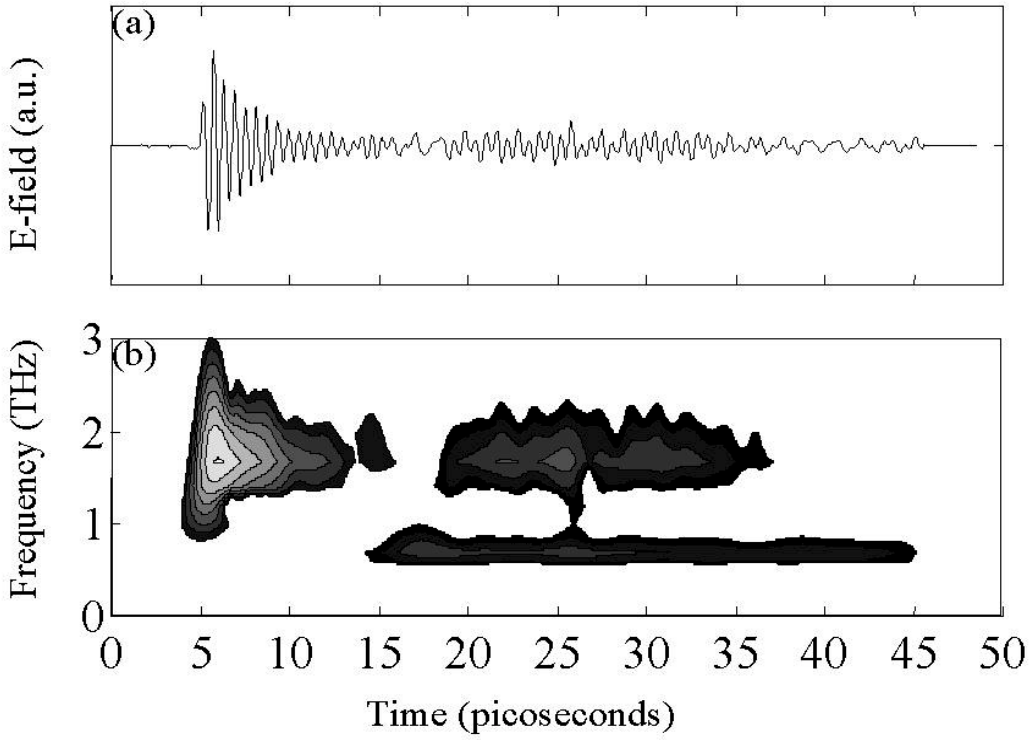

Figure 4: (a) Trace of the THz wave over a long time window; (b) Time-frequency wavelet spectrogram. Brighter areas correspond to higher powers.

To determine the power and spectral brightness of the THz field, we measured the radiated field with a bolometer. For a 400 nJ pulse, we measure approximately 1.5 μW of THz power at low temperature from the 1.2 mm PPLN. This corresponds to a spectral brightness of approximately 20 μW/THz in the 1.75-1.85 THz frequency range, as compared to approximately 0.5 μW/THz for the same frequency range in ZnTe. When focused to a spot size of 300 microns, the peak electric field for our THz pulse is on the order of 8 x 10^4 V/m.

4. Modeling the THz field

To solve for the radiated field, we must first calculate the polarization as a function of position and time in the crystal. For a tractable result, we assume a gaussian plane-wave pulse propagating in the z direction of a dispersionless medium:

$$E(z,t) = E_0 \exp[i(\omega_0 t - k_0 z) \exp[-((t - z/v_g)/\tau_p)^2/2] \quad (8)$$

where v_g is the group velocity of the optical pulse, c/n_{opt}, _0 is the center frequency of the optical carrier, k_0 is its propagation constant, and E_0 is the peak field. In principle, we use this pulse shape as the source of our polarization in equation (4), and then solve equation (3) for the THz frequency field. In practice, however, direct time-domain solutions are difficult to calculate; the problem become much more manageable under Fourier transformation to the frequency domain. The wave equation in the frequency domain becomes an inhomogeneous Helmholtz equation:

$$\left(\frac{\partial^2}{\partial z^2} + n^2(\omega)\frac{\omega^2}{c^2}\right)E(z,\omega) = -\mu_0\omega^2 P(z,\omega) \quad (9)$$

In equation (9), n(_) is the complex refractive index, and we have already accounted for the linear part of the polarization, so that here, $P(z,\_)$ is only the nonlinear polarization. A convenient way to solve this equation is by the method of Green s functions. Because Green s functions for the Helmholtz equation are well-known [18], and the case of an optical rectification inhomogeneity has also been studied in detail [19,20], we will simply give the results of the calculation. At the back surface of the crystal ($z' = L$), the radiated field from each position, z', is:

$$E(z',\omega) \propto \chi^{(2)}(z',\omega)\omega^2 \exp[-(\omega\tau_p/2)^2 - i\omega\{(n_{opt} - n_{THz})z'/c + Ln_{THz}/c\}] \quad (10)$$

This equation may then be Fourier transformed back to the time domain, and integrated over the crystal to yield the measured THz signal as a function solely of time.

Simulations of the THz field are shown in figure 5. Figures 5(a) and (b) are the time domain and power spectrum simulations, respectively, and include a THz absorption term. When the absorption term is included in the THz index, we attain very good agreement between our calculated field and our measured field at room temperature. The spectrum shown in 5(b) is peaked at 1.72 THz and has a bandwidth of 0.10 THz. For the low temperature data, no such absorption term is needed to model the data accurately, as in figures 5(c) and (d). The spectrum in figure 5(d) is also peaked at 1.72 THz (we did not account for index changes and crystal contraction at low temperatures in the simulation), and has a bandwidth of 0.08 THz.

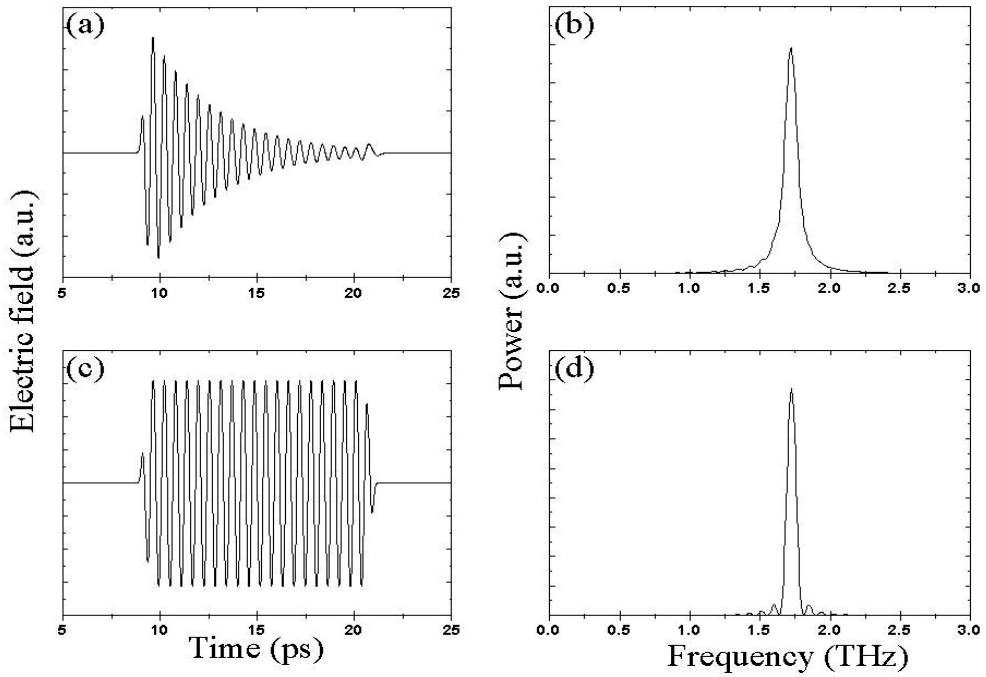

Figure 5: Numerical simulations of the THz field, with absorption (a, b), and without absorption (c, d).

5. Summary & future prospects

Research into generation of narrow-bandwidth THz sources has been vigorous recently. Photomixing on THz antennas offers a usable source of continuous wave THz, but antenna response severely limits the power available from such devices on the high-frequency end [21]. Other research has focused on pulse-shaping techniques. To limit the radiated bandwidth, pulse-shapers for the optical beam [22,23] and also for the THz signal itself [24] have been demonstrated. Pulse-shaping, however, is intrinsically inefficient. In contrast to these methods, we demonstrate a method for generating narrow-bandwidth THz by engineering the nonlinear crystal itself to produce the desired waveform.

Ultimately, we anticipate that other poled materials will surpass PPLN as a medium for THz waveform generation. Poled polymers have large nonlinear coefficients [25], and could provide a strong THz system if they are able to be periodically-poled. For spectroscopic and sensing applications, chirped poled media (i.e. poled so that the domain size increases as one moves laterally across the crystal) could be an extremely useful source of tunable THz radiation.

In summary, we have shown that optical rectification of a femtosecond pulse in a periodically-poled lithium niobate crystal gives rise to a THz waveform which largely

depends on the domain structure of the poled crystal. In particular, narrow bandwidth waveforms may be achieved by a proper choice of domain length in a periodic crystal.

6. References

1. P.A. Franken, A.E. Hill, C.W. Peters, and G. Weinreich, Phys. Rev. Lett., **7**, 118 (1961).
2. R.W. Boyd, *Nonlinear Optics*, Academic Press, San Diego, 1992.
3. A. Yariv, and P. Yeh, *Optical Waves in Crystals*, Wiley, New York, 1984.
4. A. Bonvalet, M. Joffre, J.L. Martin, and A. Migus, Appl. Phys. Lett., **67**, 2907 (1995).
5. A. Nahata, A.S. Weling, and T.F. Heinz, Appl. Phys. Lett., **69**, 2321 (1996).
6. U. Peschel, K. Bubke, D.C. Hitchings, J.S. Aitchison, and J.M. Arnold, Phys. Rev. A, **60**, 4918 (1999).
7. L.E. Myers, R.C. Eckardt, M.M. Fejer, R.L. Byer, W.R. Bosenberg, and J.W. Pierce, J. Opt. Soc. Am. B, **12**, 2102 (1995).
8. Y.-S. Lee, T. Meade, V. Perlin, H. Winful, T.B. Norris, and A. Galvanauskas, Appl. Phys. Lett., **76**, 2505 (2000).
9. T.B. Norris, Opt. Lett., **17**, 1009 (1992).
10. H.J. Bakker, S. Hunsche, and H. Kurz, Phys. Rev. B, **50**, 914 (1994).
11. B.H. Kolner and D.M. Bloom, IEEE J. Quantum Electron., **22**, 69 (1986).
12. J.A. Valdmanis and G.A. Mourou, IEEE J. Quantum Electron., **22**, 79 (1986).
13. Q. Wu and X.-C. Zhang, Appl. Phys. Lett., **67**, 3523 (1995).
14. Q. Wu and X.-C. Zhang, Appl. Phys. Lett., **68**, 1604 (1996).
15. H. Ito, K. Kawase, and J. Shikata, IEICE Trans. Electron., **E81-C**, 264 (1998).
16. C. Torrence and G.P. Compo, Bull. Am. Meteorol. Soc., 79, 61 (1998).
17. Wavelet software provided by C. Torrence and G.P. Compo, and is available at http://paos.colorado.edu/research/wavelets
18. J.D. Jackson, *Classical Electrodynamics*, Wiley, New York, 1975.
19. D.H. Auston and M.C. Nuss, IEEE J. Quantum Eletron., **QE-24**, 184 (1988).
20. C. Kolleck, J. Opt. Soc. Am. B, **16**, 1250 (1999).
21. E.R. Brown, K.A. McIntosh, K.B. Nichols, and C.L. Dennis, Appl. Phys. Lett., **66**, 285 (1995).
22. Y.Q. Liu, S.G. Park, and A.M. Weiner, IEEE J. Sel. Top. Quantum Electron., **2**, 709 (1996).
23. C. Messner, M. Sailer, H. Kostner, and R.A. H pfel, Appl. Phys. B, **64**, 619 (1997).
24. J. Bromage, S. Radic, G.P. Agrawal, C.R. Stroud, P.M. Fauchet, and R. Sobolewski, Opt. Lett., **22**, 627 (1997).
25. A. Nahata, D.H. Auston, C. Wu, and J.T. Yardley, Appl. Phys. Lett., **67**, 1358 (1995).